Research Article | Vol. 25, No. 25 | 11 Dec 2017 | OPTICS EXPRESS 31758
Optics EXPRESS

Low loss GaN waveguides at the visible spectral wavelengths for integrated photonics applications

HONG CHEN, HOUQIANG FU, XUANQI HUANG, XIAODONG ZHANG, TSUNG-HAN YANG, JOSSUE A. MONTES, IZAK BARANOWSKI, AND YUJI ZHAO*

School of Electrical, Computer and Energy Engineering, Arizona State University, Tempe, AZ 85287, USA
**yuji.zhao@asu.edu*

Abstract: We perform comprehensive studies on the fundamental loss mechanisms in III-nitride waveguides in the visible spectral region. Theoretical analysis shows that free carrier loss dominates for GaN under low photon power injection. When optical power increases, the two photon absorption loss becomes important and eventually dominates when photon energy above half-bandgap of GaN. When the dimensions of the waveguides reduce, the sidewall scattering loss will start to dominate. To verify the theoretical results, a high performance GaN-on-sapphire waveguide was fabricated and characterized. Experimental results are consistent with the theoretical findings, showing that under high power injection the optical loss changed significantly for GaN waveguides. A low optical loss ~2 dB/cm was achieved on the GaN waveguide, which is the lowest value ever reported for the visible spectral range. The results and fabrication processes developed in this work pave the way for the development of III-nitride integrated photonics in the visible and potentially ultraviolet spectral range for nonlinear optics and quantum photonics applications.

OCIS codes: (130.0130) Integrated optics; (190.4180) Multiphoton processes; (160.3130) Integrated optics materials.

References and links

1. S. Pimputkar, J. S. Speck, S. P. DenBaars, and S. Nakamura, "Prospects for LED lighting," Nat. Photonics **3**(4), 180–182 (2009).
2. Y. Zhao, S. Tanaka, C. C. Pan, K. Fujito, D. Feezell, J. S. Speck, S. P. DenBaars, and S. Nakamura, "High-power blue-violet semipolar (2021) InGaN/GaN light-emitting diodes with low efficiency droop at 200 A/cm2," Appl. Phys. Express **4**(8), 082104 (2011).
3. S. Nakamura, M. Senoh, S. I. Nagahama, N. Iwasa, T. Yamada, T. Matsushita, H. Kiyoku, and Y. Sugimoto, "InGaN-based multi-quantum-well-structure laser diodes," Jpn. J. Appl. Phys. **35**(1B), L74 (1996).
4. S. P. DenBaars, D. Feezell, K. Kelchner, S. Pimputkar, C. C. Pan, C. C. Yen, S. Tanaka, Y. Zhao, N. Pfaff, R. Farrell, and M. Iza, "Development of gallium-nitride-based light-emitting diodes (LEDs) and laser diodes for energy-efficient lighting and displays," Acta Mater. **61**(3), 945–951 (2013).
5. T. Nishida, H. Saito, and N. Kobayashi, "Efficient and high-power AlGaN-based ultraviolet light-emitting diode grown on bulk GaN," Appl. Phys. Lett. **79**(6), 711–712 (2001).
6. Y. Zhao, S. H. Oh, F. Wu, Y. Kawaguchi, S. Tanaka, K. Fujito, J. S. Speck, S. P. DenBaars, and S. Nakamura, "Green semipolar (2021) InGaN light-emitting diodes with small wavelength shift and narrow spectral linewidth," Appl. Phys. Express **6**(6), 062102 (2013).
7. C. Xiong, W. Pernice, K. K. Ryu, C. Schuck, K. Y. Fong, T. Palacios, and H. X. Tang, "Integrated GaN photonic circuits on silicon (100) for second harmonic generation," Opt. Express **19**(11), 10462–10470 (2011).
8. W. M. Green, M. J. Rooks, L. Sekaric, and Y. A. Vlasov, "Ultra-compact, low RF power, 10 Gb/s silicon Mach-Zehnder modulator," Opt. Express **15**(25), 17106–17113 (2007).
9. J. F. Muth, J. D. Brown, M. A. L. Johnson, Z. Yu, R. M. Kolbas, J. W. Cook, Jr., and J. F. Schetzina, "Absorption coefficient and refractive index of GaN, AlN and AlGaN alloys," MRS Internet J. Nitride Semicond. Res. **4**(S1), G5.2 (1999).
10. G. M. Laws, E. C. Larkins, I. Harrison, C. Molloy, and D. Somerford, "Improved refractive index formulas for the Al x Ga 1– x N and In y Ga 1– y N alloys," J. Appl. Phys. **89**(2), 1108–1115 (2001).
11. J. L. Hughes, Y. Wang, and J. E. Sipe, "Calculation of linear and second-order optical response in wurtzite GaN and AlN," Phys. Rev. B **55**(20), 13630 (1997).

#308457 https://doi.org/10.1364/OE.25.031758
Journal © 2017 Received 3 Oct 2017; revised 26 Nov 2017; accepted 28 Nov 2017; published 6 Dec 2017

Optics EXPRESS

12. X. Guo, C. L. Zou, and H. X. Tang, "Second-harmonic generation in aluminum nitride microrings with 2500%/W conversion efficiency," Optica **3**(10), 1126–1131 (2016).
13. C. Xiong, W. H. Pernice, X. Sun, C. Schuck, K. Y. Fong, and H. X. Tang, "Aluminum nitride as a new material for chip-scale optomechanics and nonlinear optics," New J. Phys. **14**(9), 095014 (2012).
14. X. Guo, C. L. Zou, H. Jung, and H. X. Tang, "On-chip strong coupling and efficient frequency conversion between telecom and visible optical modes," Phys. Rev. Lett. **117**(12), 123902 (2016).
15. H. Jung, R. Stoll, X. Guo, D. Fischer, and H. X. Tang, "Green, red, and IR frequency comb line generation from single IR pump in AlNmicroring resonator," Optica **1**(6), 396–399 (2014).
16. X. Liu, C. Sun, B. Xiong, L. Wang, J. Wang, Y. Han, Z. Hao, H. Li, Y. Luo, J. Yan, and T. Wei, "Nearly octave-spanning frequency comb generation in AlN-on-sapphire microresonators," arXiv:**1611**, 01994 (2016).
17. M. Soltani, R. Soref, T. Palacios, and D. Englund, "AlGaN/AlN integrated photonics platform for the ultraviolet and visible spectral range," Opt. Express **24**(22), 25415–25423 (2016).
18. D. Y. Oh, D. Sell, H. Lee, K. Y. Yang, S. A. Diddams, and K. J. Vahala, "Supercontinuum generation in an on-chip silica waveguide," Opt. Lett. **39**(4), 1046–1048 (2014).
19. R. Claps, D. Dimitropoulos, V. Raghunathan, Y. Han, and B. Jalali, "Observation of stimulated Raman amplification in silicon waveguides," Opt. Express **11**(15), 1731–1739 (2003).
20. X. Liu, C. Sun, B. Xiong, L. Wang, J. Wang, Y. Han, Z. Hao, H. Li, Y. Luo, J. Yan, and T. Wei, "Integrated continuous-wave aluminum nitride Raman laser," Optica **4**(8), 893–896 (2017).
21. H. Chen, X. Huang, H. Fu, Z. Lu, X. Zhang, J. A. Montes, and Y. Zhao, "Characterizations of nonlinear optical properties on GaN crystals in polar, nonpolar, and semipolar orientations," Appl. Phys. Lett. **110**(18), 181110 (2017).
22. R. A. Soref and B. R. Bennett, "Electrooptical effects in silicon," IEEE J. Quantum Electron. **23**, 123–129 (1987).
23. R. Hui, S. Taherion, Y. Wan, J. Li, S. X. Jin, J. Y. Lin, and H. X. Jiang, "GaN-based waveguide devices for long-wavelength optical communications," Appl. Phys. Lett. **82**(9), 1326–1328 (2003).
24. A. Stolz, E. Cho, E. Dogheche, Y. Androussi, D. Troadec, D. Pavlidis, and D. Decoster, "Optical waveguide loss minimized into gallium nitride based structures grown by metal organic vapor phase epitaxy," Appl. Phys. Lett. **98**(16), 161903 (2011).
25. S. C. Mao, S. H. Tao, Y. L. Xu, X. W. Sun, M. B. Yu, G. Q. Lo, and D. L. Kwong, "Low propagation loss SiN optical waveguide prepared by optimal low-hydrogen module," Opt. Express **16**(25), 20809–20816 (2008).
26. K. K. Lee, D. R. Lim, L. C. Kimerling, J. Shin, and F. Cerrina, "Fabrication of ultralow-loss Si/SiO2 waveguides by roughness reduction," Opt. Lett. **26**(23), 1888–1890 (2001).
27. R. J. Deri and E. Kapon, "Low-loss III-V semiconductor optical waveguides," IEEE J. Quantum Electron. **27**(3), 626–640 (1991).
28. N. Daldosso, M. Melchiorri, F. Riboli, F. Sbrana, L. Pavesi, G. Pucker, C. Kompocholis, M. Crivellari, P. Bellutti, and A. Lui, "Fabrication and optical characterization of thin two-dimensional Si 3 N 4 waveguides," Mater. Sci. Semicond. Process. **7**(4), 453–458 (2004).
29. H. Chen, H. Fu, X. Huang, Z. Lu, X. Zhang, J. Montes, and Y. Zhao, "Optical Cavity Effects in InGaN Micro-Light-Emitting Diodes With Metallic Coating," IEEE Photonics J. **9**(3), 1–8 (2017).
30. A. W. Bruch, C. Xiong, B. Leung, M. Poot, J. Han, and H. X. Tang, "Broadband nanophotonic waveguides and resonators based on epitaxial GaN thin films," Appl. Phys. Lett. **107**(14), 141113 (2015).
31. S. Keller, G. Parish, P. T. Fini, S. Heikman, C. H. Chen, N. Zhang, S. P. DenBaars, U. K. Mishra, and Y. F. Wu, "Metalorganic chemical vapor deposition of high mobility AlGaN/GaN heterostructures," J. Appl. Phys. **86**(10), 5850–5857 (1999).
32. R. J. Shul, G. C. McClellan, S. A. Casalnuovo, D. J. Rieger, S. J. Pearton, C. Constantine, C. Barratt, R. F. Karlicek, Jr., C. Tran, and M. Schurman, "Inductively coupled plasma etching of GaN," Appl. Phys. Lett. **69**(8), 1119–1121 (1996).
33. P. K. Tien, "Light waves in thin films and integrated optics," Appl. Opt. **10**(11), 2395–2413 (1971).
34. Y. Vlasov and S. McNab, "Losses in single-mode silicon-on-insulator strip waveguides and bends," Opt. Express **12**(8), 1622–1631 (2004).
35. C. G. Poulton, C. Koos, M. Fujii, A. Pfrang, T. Schimmel, J. Leuthold, and W. Freude, "Radiation modes and roughness loss in high index-contrast waveguides," IEEE J. Sel. Top. Quantum Electron. **12**(6), 1306–1321 (2006).
36. J. Lacey and F. Payne, "Radiation loss from planar waveguides with random wall imperfections," IEE Proc. J. **137**, 282–288 (1990).
37. M. Sheik-Bahae, D. C. Hutchings, D. J. Hagan, and E. W. Van Stryland, "Dispersion of bound electron nonlinear refraction in solids," IEEE J. Quantum Electron. **27**(6), 1296–1309 (1991).
38. C. K. Sun, J. C. Liang, J. C. Wang, F. J. Kao, S. Keller, M. P. Mack, U. Mishra, and S. P. DenBaars, "Two-photon absorption study of GaN," Appl. Phys. Lett. **76**(4), 439–441 (2000).
39. D. Zhuang and J. H. Edgar, "Wet etching of GaN, AlN, and SiC: a review," Mater. Sci. Eng. R-Rep. **48**(1), 1–46 (2005).
40. C. Gupta, Y. Enatsu, G. Gupta, S. Keller, and U. K. Mishra, "High breakdown voltage p–n diodes on GaN on sapphire by MOCVD," Phys. Status Solidi., A Appl. Mater. Sci. **213**(4), 878–882 (2016).

Optics EXPRESS

41. M. K. Kelly, R. P. Vaudo, V. M. Phanse, L. Görgens, O. Ambacher, and M. Stutzmann, "Large free-standing GaN substrates by hydride vapor phase epitaxy and laser-induced liftoff," Jpn. J. Appl. Phys. **38**(3A), 217 (1999).
42. M. Funato, M. Ueda, Y. Kawakami, Y. Narukawa, T. Kosugi, M. Takahashi, and T. Mukai, "Blue, green, and amber InGaN/GaN light-emitting diodes on semipolar {11-22} GaN bulk substrates," Jpn. J. Appl. Phys. **45**(7L), 659 (2006).
43. K. Misiakos, and D. Tsamakis, "Accurate measurements of the silicon intrinsic carrier density from 78 to 340 K," J. Appl. Phys. **74**(5), 3293–3297 (1993).
44. S. M. Sze and K. K. Ng, "Physics of semiconductor devices." John wiley & sons (2006).
45. K. Kainosho, H. Shimakura, H. Yamamoto, and O. Oda, "Undoped semi-insulating InP by high-pressure annealing," Appl. Phys. Lett. **59**(8), 932–934 (1991).
46. O. Malyk, "Charge carrier mobility in gallium nitride," Diamond Related Materials **23**, 23–27 (2012).
47. M. E. Levinshtein, S. L. Rumyantsev, and M. S. Shur, *Properties of Advanced Semiconductor Materials: GaN, AIN, InN, BN, SiC, SiGe* (John Wiley & Sons 2001).
48. W. Li, D. Ji, R. Tanaka, S. Mandal, M. Laurent, and S. Chowdhury, "Demonstration of GaN Static Induction Transistor (SIT) Using Self-Aligned Process," IEEE J. Electron Devices Soc. **5**(6), 485–490 (2017).
49. S. McNab, N. Moll, and Y. Vlasov, "Ultra-low loss photonic integrated circuit with membrane-type photonic crystal waveguides," Opt. Express **11**(22), 2927–2939 (2003).
50. T. Sekiya, T. Sasaki, and K. Hane, "Design, fabrication, and optical characteristics of freestanding GaN waveguides on silicon substrate," J. Vac. Sci. Technol. B **33**(3), 031207 (2015).
51. W. Li, Y. Luo, B. Xiong, C. Sun, L. Wang, J. Wang, Y. Han, J. Yan, T. Wei, and H. Lu, "Fabrication of GaN-based ridge waveguides with very smooth and vertical sidewalls by combined plasma dry etching and wet chemical etching," Phys. Status Solidi., A Appl. Mater. Sci. **212**(10), 2341–2344 (2015).
52. R. Geiss, A. Chowdhury, C. M. Staus, H. M. Ng, S. S. Park, and J. Y. Han, "Low loss GaN at 1550 nm," Appl. Phys. Lett. **87**(13), 132107 (2005).
53. M. Gromovyi, F. Semond, J. Y. Duboz, G. Feuillet, and M. P. De Micheli, "Low loss GaN waveguides for visible light on Si substrates," J. Eur. Opt. Soc. **9**, 14050 (2014).

1. Introduction

GaN-based III-nitride semiconductors have achieved great success in the fabrication of active optical devices such as light-emitting diodes (LEDs) [1,2] and lasers diodes [3,4], where they showed high radiative efficiency at the visible wavelengths, a spectral range that is unattainable using other materials [5,6]. For passive optical devices such as waveguides, resonators [7], and modulators [8], III-nitride materials are also expected to produce high performance devices especially at the visible and ultraviolet (UV) wavelengths due to their outstanding optical properties such as wide bandgaps (i.e., transparent at the visible and UV spectral range), low dispersion [9,10], active integration capability, and second order susceptibility [11,12]. Despite these advantages, however, the majority interests of the integrated photonics society have been focused on 1.55 μm wavelengths based on III-V or Si materials for fiber optics applications, with only very limited experimental work on GaN passive optical devices such as photonic waveguides.

Recent progress on UV and visible integrated photonics [12–18] have opened up new opportunities for III-nitride photonics in applications such as biochemical sensing, Raman spectroscopy, beam steering, nonlinear optics, and quantum photonics. For these applications, a high-power density pumping is typically required for various III-nitride waveguide structures. For example, applications such as stimulated Raman scattering, comb generation, and super continuum generation will require pumping power on the order of hundreds of milliwatts inside the waveguides [15–20]. For other threshold-less process such as second harmonic generation and entangled photon generation, the power of the signals is typically proportional to the square of incident power, which could be on the order of tens to hundreds of milliwatts [7,12,14]. These applications will therefore require high performance III-nitride waveguides with extremely low optical loss, which presents a major technical challenge. In contrast to traditional photonic waveguides (e.g., Si or III-V) at 1.55 μm where the optical loss is mainly due to the sidewall scattering effects, the performance of GaN waveguide at the visible spectral wavelength is dominated by several different loss mechanisms. First, under high power operation the optical loss of III-nitride waveguides is dominated by multi-photon absorption process [21]. Second, grain boundaries formed in GaN material grown on sapphire

Optics EXPRESS

typically show different etching speeds during dry etching, which degrades the side wall roughness and hence introduces additional loss to GaN waveguides. Furthermore, due to the material epitaxial processes, III-nitride materials are intrinsically n-type doped, which will also lead to large free carrier loss to III-nitride waveguides. Since the free carrier loss is proportional to the inverse of carrier mobility [22], the material quality of III-nitride material (e.g., dislocation density) will have a strong impact on the waveguide performance. In this work, we performed comprehensive studies on the loss mechanisms in III-nitride GaN waveguide devices. A high performance GaN waveguide with extremely low optical loss of ~2 dB/cm was achieved, which can pave the way for various III-nitride integrated photonics applications.

This paper is organized as the following: In Section 2, we describe a theoretical analysis on the optical losses in III-nitride waveguides for GaN-on-sapphire structures. Scattering loss, free carrier loss, and two-photon absorption (TPA) loss will be studied, and their contributions to the overall performance of waveguide devices will be discussed. In Section 3, we describe the fabrication and characterization processes for GaN-on-sapphire waveguides. A high performance GaN waveguide with optical loss as low as ~2dB/cm is achieved above half bandgap energy (λ < 770 nm), which is the lowest value ever reported for GaN waveguides [23,24], comparable to state-of-the-art low loss Si/III-V waveguide devices at the 1.55 μm wavelengths [25–28].

2. Theoretical analysis

2.1 Method

In order to analyze scattering loss, free carrier loss, and TPA loss in III-nitride ridge waveguides, we first calculated the wave vectors and optical modes in the waveguides. A commercial software package by Lumerical Mode Solutions was implemented in this work, and the simulation setup is similar to our previous work [29].We focused on the GaN waveguide as it has the most promising properties for visible spectral range [1–6,17]. The substrate of the simulation was chosen to be sapphire which is the most commonly used material for III-nitride epitaxial growth. Sapphire also provides sufficient optical confinement and is transparent at visible wavelengths. The schematic for the GaN-on-sapphire waveguide is shown in Fig. 1(a), in which W and H indicate waveguide width and height, respectively. To simplify our discussion, W and H are equal throughout the analysis and their values vary from 0.1 μm to 1.6 μm. In order to study the wavelength dependence, modes at 1550 nm, 800 nm, 600 nm, and 400 nm are simulated, in which 1550 nm represents the telecommunication wavelength, 800 nm represents the wavelength of typical pulsed laser, 600 nm and 400 nm represent visible wavelengths.

For the scattering loss, we only considered sidewall roughness and neglected the upper surface roughness. This is because the III-nitride epitaxy layers usually have very smooth surface (e.g., roughness less than 1 nm [30,31]), while dry etching processes will give rise to surface roughness on the side walls which is typically on the order of several nanometers [32]. This simplification is taken in most of theoretical analysis dealing with sidewall scattering [33–36]. In this work, we used a widely discussed analytical model for scattering loss estimation, given in [33,34]. More advanced models utilizing coupled-mode techniques [35] or volume current method [36] will give higher accuracy, but that is beyond the scope of this work.

For the free carrier loss α_{FC}, we used an equation from Drude model [22]:

$$\alpha_{FC} = \frac{Ne^3}{m_e^{*2} n \varepsilon_0 \omega^2 \mu c} \tag{1}$$

Optics EXPRESS

where N indicates carrier density, m_e^* is the effective mass of electron, n is the refractive index, ω is the optical frequency, μ is the mobility. e, ε_0, and c are constants that represent elementary charge, vacuum permittivity, and speed of light, respectively.

For the TPA loss α_{TPA}, we used the following equation:

$$\alpha_{TPA} = \beta \frac{P_{in}}{A_{eff}} \tag{2}$$

where β is the TPA coefficient [21], P_{in} is the optical power inside waveguide, and A_{eff} is the mode area. We note here that for calculations on a GaN waveguide, we used β from [21], which involves a fitting parameter. This fitting parameter is a material-independent constant and typically has a larger value for wide bandgap materials such as III-nitrides. More information can be found in [37,38].

2.2 Results and discussion

2.2.1 Dispersion relation and mode area analysis

Figure 1(b) shows the calculated dispersion curves of GaN waveguides for the first order transverse electric (TE) modes with different waveguide dimensions. Similar results were also obtained for the transverse magnetic (TM) mode which are not shown here. Wave vectors β_z along the propagation direction for each mode can be obtained by using the relation: $\beta_z = n_{eff}\frac{\omega}{c}$, where n_{eff} represents the effective refractive index of each mode. At the low photon energy region, highly dispersive relations are observed for the GaN waveguides particularly in small waveguide dimensions due to the relative strong optical confinement. This dispersion is reduced with waveguide dimension and can be engineered by controlling the size of the waveguide for a variety of applications [7,12–16,18]. While at the high photon energy region, highly dispersive relations are observed for waveguides at all dimensions which is due to intrinsic material dispersion. Table 1 summarizes the cut off wavelengths for the GaN waveguides with different dimensions. Figure 1(c) shows the calculated mode areas vs. waveguide areas for GaN waveguides, where the mode areas decrease with the waveguide dimensions. A small increase of mode area is observed near the cut off, which is attributed to the slow decay of field intensity outside of the waveguide region near the cut off condition.

Table 1. The cut-off wavelengths for the GaN waveguides with different dimensions.

Wavelength	Waveguide cut off*
1550 nm	0.55 μm × 0.55 μm
800 nm	0.30 μm × 0.30 μm
600 nm	0.20 μm × 0.20 μm
400 nm	0.15 μm × 0.15 μm

Optics EXPRESS

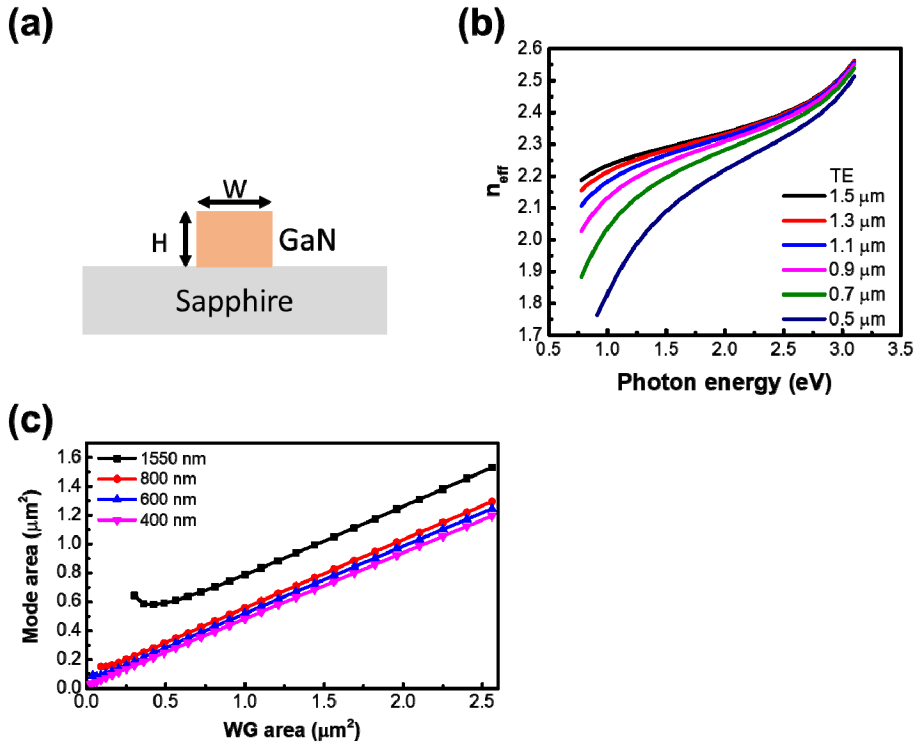

Fig. 1. (a) Schematic structures of the GaN-on-sapphire waveguides studied in this work. (b) Calculated dispersion relation of the first order TE-like mode in GaN waveguides at different waveguide cross section dimensions. (c) Calculated mode areas vs. waveguide areas for GaN waveguides at different wavelengths.

2.2.2 Scattering loss, free carrier loss, and TPA loss analysis

Scattering loss

Figure 2(a) shows calculated sidewall scattering losses vs. wavelengths for the GaN waveguides at the dimensions1.6 μm × 1.6 μm and 0.6 μm × 0.6 μm when sidewall roughness (σ) is 1 nm. Different trends were observed for two waveguides dimensions. For waveguide with 1.6 μm × 1.6 μm dimension (i.e., large waveguide dimension), a peak was observed at the 600 nm wavelength. This is because at very short wavelengths, modes are better confined inside the waveguides and interact less with the surfaces, which leads to lower scattering loss. When the wavelengths increase, the scattering loss increases due to the stronger interaction with surfaces. At very long wavelengths, however, surface roughness becomes less significant compared to the wavelengths, which lowers the scattering loss again. For waveguides at 0.6 μm × 0.6 μm dimension (i.e., small waveguide dimension), modes have more chance to interact with surface due to the relative smaller waveguides dimension. Therefore the scattering loss decreases with increasing wavelengths in this case since shorter wavelengths are more comparable to the roughness. Figure 2(b) shows the relationship between the scattering loss and the waveguide dimensions at 400 nm, 600 nm, 800 nm, and 1550 nm wavelengths, which are consistent with the results in Fig. 2(a). It was observed that as the dimension of the waveguide decreases, the optical loss increases due to the stronger optical confinement. It is also worth noting that for waveguides with dimensions above the micron scale, scattering loss becomes less significant, while at submicron dimension, scattering loss becomes more significant especially for visible light. Since sidewall roughness

Optics EXPRESS

is usually attributed to different dry etching speeds at grain boundaries, GaN samples with high material quality are important when manufacturing low loss submicron waveguides.

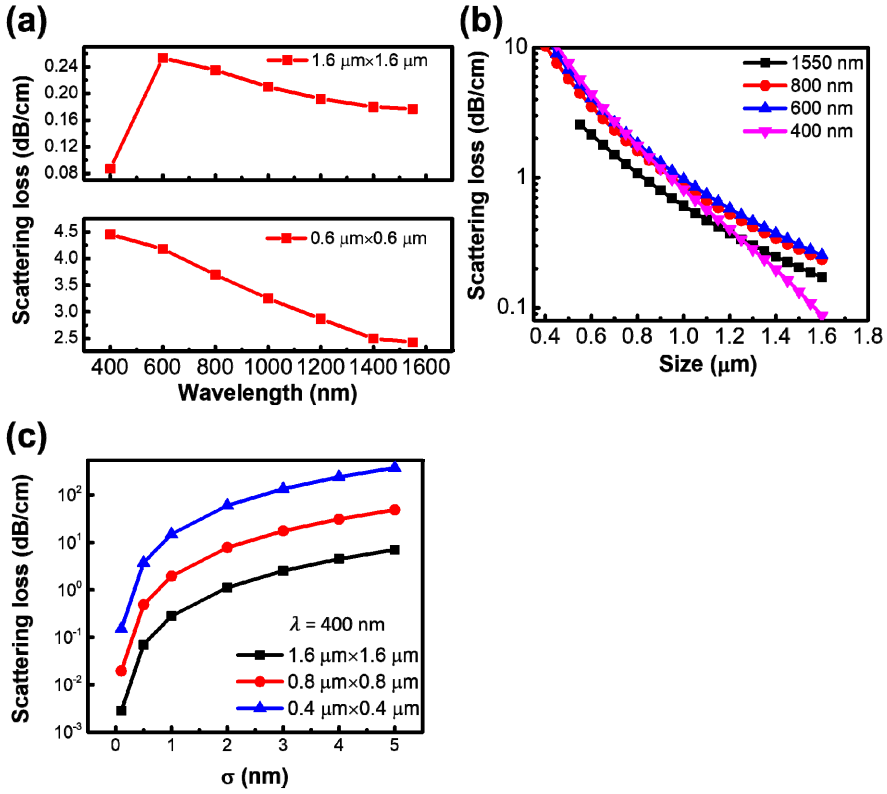

Fig. 2. (a) Calculated sidewall scattering loss vs. wavelengths for GaN waveguides with dimensions of 1.6 μm × 1.6μm and 0.6 μm × 0.6 μm. (b) Calculated sidewall scattering loss vs. waveguide with wavelengths at 400, 600, 800 and 1550 nm. Sidewall surface roughness σ used in (a) and (b) is 1 nm which represents the ideal case. (c) Calculated sidewall scattering loss vs. sidewall roughness σ at 400 nm for GaN waveguides at waveguide dimensions of 1.6 μm × 1.6μm, 0.8 μm × 0.8μm, and 0.4 μm × 0.4μm.

Figure 2(c) shows the calculated scattering loss vs. sidewall surface roughness at 400 nm for GaN waveguides with different dimensions. The scattering losses increase with the side wall roughness. Note that the sidewall roughness of GaN waveguides can be suppressed down to ~1 nm using optimized dry etching techniques [32] and post etching treatments [39]. Therefore, for micron (1.6 μm × 1.6 μm) and submicron (0.8 μm × 0.8 μm, 0.4 μm × 0.4 μm) GaN waveguides, the sidewall scattering loss can be theoretically suppressed to ~1dB/cm as shown in Fig. 2(c).

Free carrier loss

From Eq. (1) it can be seen that the free carrier loss is proportional to N/μ, where N is the carrier density and μ is the carrier mobility. Since III-nitride materials are intrinsically n-type doped due to the material epitaxy processes (unlike other semiconductor materials such as GaAs, InP, and Si), they typically possess a large amount of n-type free carriers which will contribute to free carrier loss. For example, the n-type carrier density for unintentionally doped GaN is on order of 10^{17} cm^{-3} for GaN epilayers grown on foreign substrates such as sapphire [40], and on order of 10^{15} to 10^{17} cm^{-3} for GaN epilayers grown on GaN bulk substrate [41,42]. These values are significantly higher than other semiconductors such as Si

Optics EXPRESS

(10^{10} cm^{-3} [43]), GaAs (10^{6} cm^{-3} [44]), and InP (10^{7} cm^{-3} [45]). Furthermore, due to the limitation of current epitaxy technology, III-nitride materials are typically grown on foreign substrates such as sapphire or SiC, which results in a high dislocation density inside the III-nitride materials. The large amount of dislocations will reduce the carrier mobility, which will further increase the free carrier loss [46]. Figure 3 shows calculated intrinsic free carrier loss vs. wavelengths for GaN waveguides at dimension of 1.6 μm × 1.6 μm. To analyze loss contributed from free carrier absorption, two cases (ideal case and practical case) were studied and compared. The redline shows the ideal case, where the carrier density of GaN is chosen to be $N_0 = 10^{15}$ cm^{-3}, which is a typical number in commercialized bulk GaN substrate [41], the corresponding n-type carrier mobility is chosen to be μ = 1800 cm^2/Vs, which was reported for high quality GaN materials with low dislocation density [46]. While black line indicates a practical case when $N/\mu = 10^3 N_0/\mu_0$, which represents the case of GaN materials grown on sapphire (typically has a high defect density of 10^9 cm^{-2}), where we picked N/μ to be 10^3 times higher than that in ideal case. The electron effective mass used in Eq. (1) is $0.2m_e$ [47], where m_e refers to the electron mass. Overall it is observed that for GaN waveguides, the free carrier loss decreases with wavelengths, indicating that the free carrier loss is less significant for GaN wavelengths at short wavelengths such as visible spectral range. In the ideal case, free carrier loss is almost negligible from 400 nm to 1600 nm. In the practical case, free carrier loss becomes larger than 1 dB/cm when the wavelengths are greater than 800 nm. These results show that GaN waveguides are more suitable to work at wavelength that shorter than 1 μm.

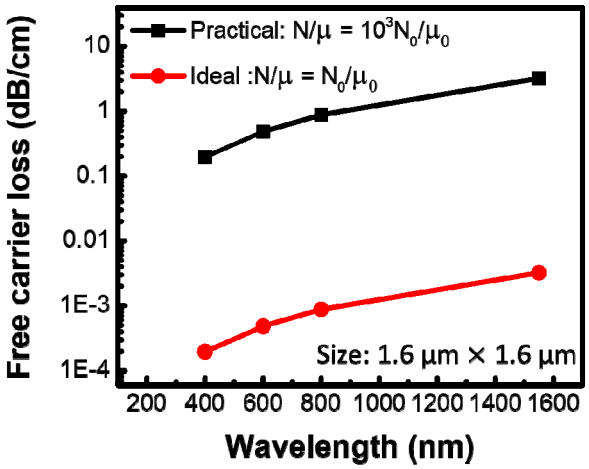

Fig. 3. Calculated free carrier loss vs. wavelength for GaN waveguides at waveguide dimensions of 1.6 μm × 1.6 μm. The redline shows the ideal case (e.g., GaN on bulk GaN substrate), while black line indicates a practical case (e.g., GaN on sapphire substrate).

Optics EXPRESS

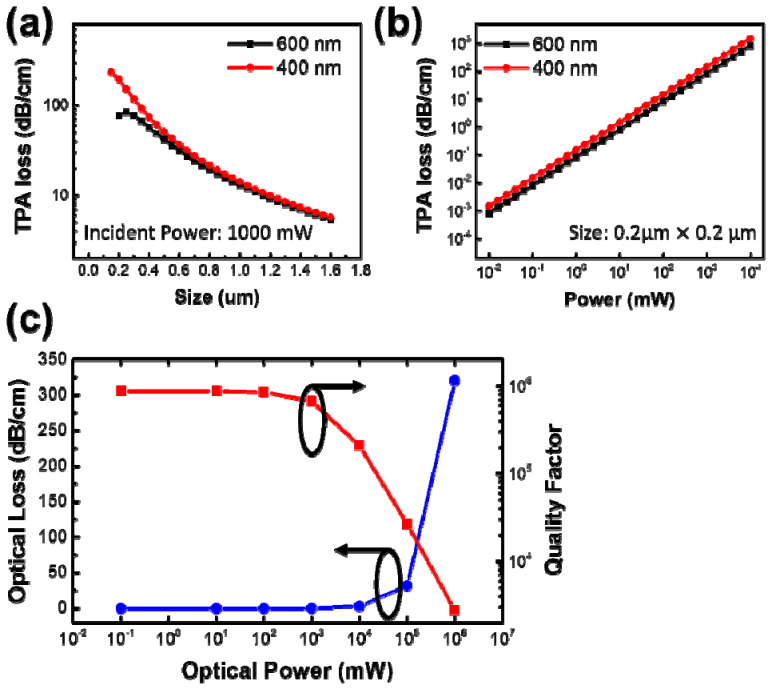

Fig. 4. (a) Calculated TPA loss vs. waveguide dimensions for GaN waveguides at different wavelengths. (b) Calculated TPA loss vs. incident power for GaN waveguides (dimension of 200 nm × 200 nm) at different wavelengths. (c) Calculated TPA loss (blue curve) and quality factor (red curve) vs. incident power for GaN waveguide using a mode area of 1 μm^2 at a wavelength of 710 nm.

TPA loss

Figure 4(a) shows calculated TPA loss vs. waveguide dimensions for GaN waveguides at different wavelengths. At a fixed power density (e.g., 1000 mW), the TPA loss will decrease with waveguide dimensions due to increased energy densities. (We also note there that the optical power simulated in Fig. 4(a) is very practical in comb generation [15,16] and super continuum generations [18]). Figure 4(b) shows calculated TPA loss vs. incident power for GaN waveguides (dimension of 200 nm × 200 nm) at different wavelengths, where the TPA loss shows a linear dependence on the incident power for simulated GaN waveguides. The TPA loss will be < 1dB/cm for when the incident power is < 10 mW, and > 10 dB/cm when the incident power is > 100 mW.

Using the TPA coefficient data, we also estimated the quality factor for the waveguides at different incident power, and the results are shown in Fig. 4(c). The calculation is based on incident wavelengths of 710 nm, which locates at the half bandgap energy of the GaN material. The mode area used in this calculation is 1 μm^2.The results show that quality factor Q remains constant when the incident optical power is low (e.g., < 1000 mW), and then drops dramatically when the incident power > 1000 mW. The TPA loss showed the opposite trend. This result implies that, on one hand, for waveguide applications under CW light operation, GaN waveguide-based ring resonators have decent performance since its quality factor drops above 1000 mW. While on the other hand, since a 1000 mW power density is very practical for waveguide applications under pulsed light operations, the quality factor drop at high power range could limit GaN-based ring resonators' applications in ultrafast optics where peak power density is usually above 1000 mW.

Optics EXPRESS

2.2.3 Overall waveguide performance analysis

With the calculation results from the previous section, we can further analyze the overall performance of GaN waveguides. At the telecom wavelength (i.e., 1550 nm), the GaN waveguide will have very poor performance mainly due to the large free carrier loss. In contrast, GaN waveguides show much higher performance at the visible wavelength (i.e., 400 – 600 nm). Figure 5 shows the calculated loss map of GaN waveguide at 600 nm with a more ideal material quality and low sidewall surface roughness (σ = 0.1 nm). At 600 nm, the total optical loss of GaN waveguide will exceed 10 dB/cm when optical power is larger than 1000 mW. The results indicate that GaN waveguides will perform best for micro waveguide and small power applications such as modulators and inter-chip connections. While for high power applications such as comb generation, second harmonic generation, stimulated Raman scattering, super continuum generation, etc., GaN waveguides can only be implemented below half-bandgap photon energy, i.e., wavelengths > 710 nm, to achieve high performance and low loss.

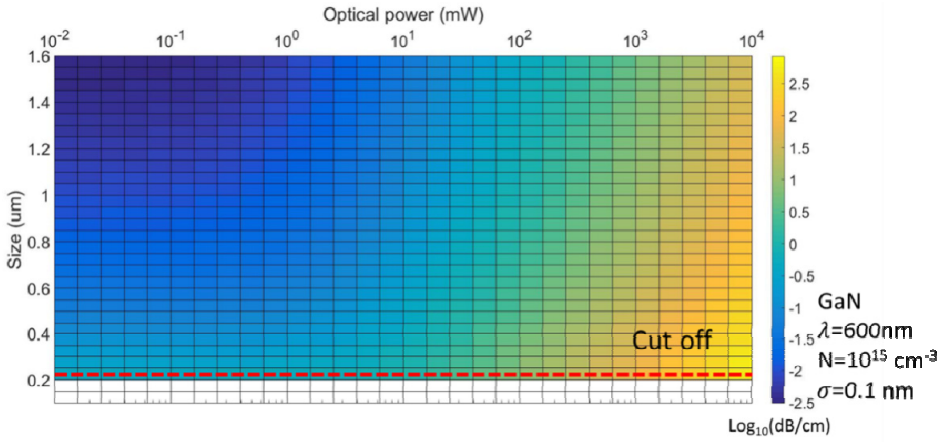

Fig. 5. Calculated loss map of GaN waveguides at 600 nm in an ideal case, i.e., good material quality (N = 10^{15} cm^{-3}) and small sidewall surface roughness (σ = 0.1 nm). The dashed line in this plot refers to cut off.

We also analyzed a more realistic case for GaN waveguide with moderate material quality $N/\mu = 10^3 N_0/\mu_0$, and sidewall roughness σ = 1 nm, and the result is shown in Figs. 6(a) and 6(b). Due to the n-type conductivity of GaN materials, the free carrier loss dominates at the low incident optical power range, which is very different from Si or InP waveguides where the scattering loss dominates. Therefore, special attention must be paid in controlling the free carrier loss when designing and fabricating GaN waveguides.

Optics EXPRESS

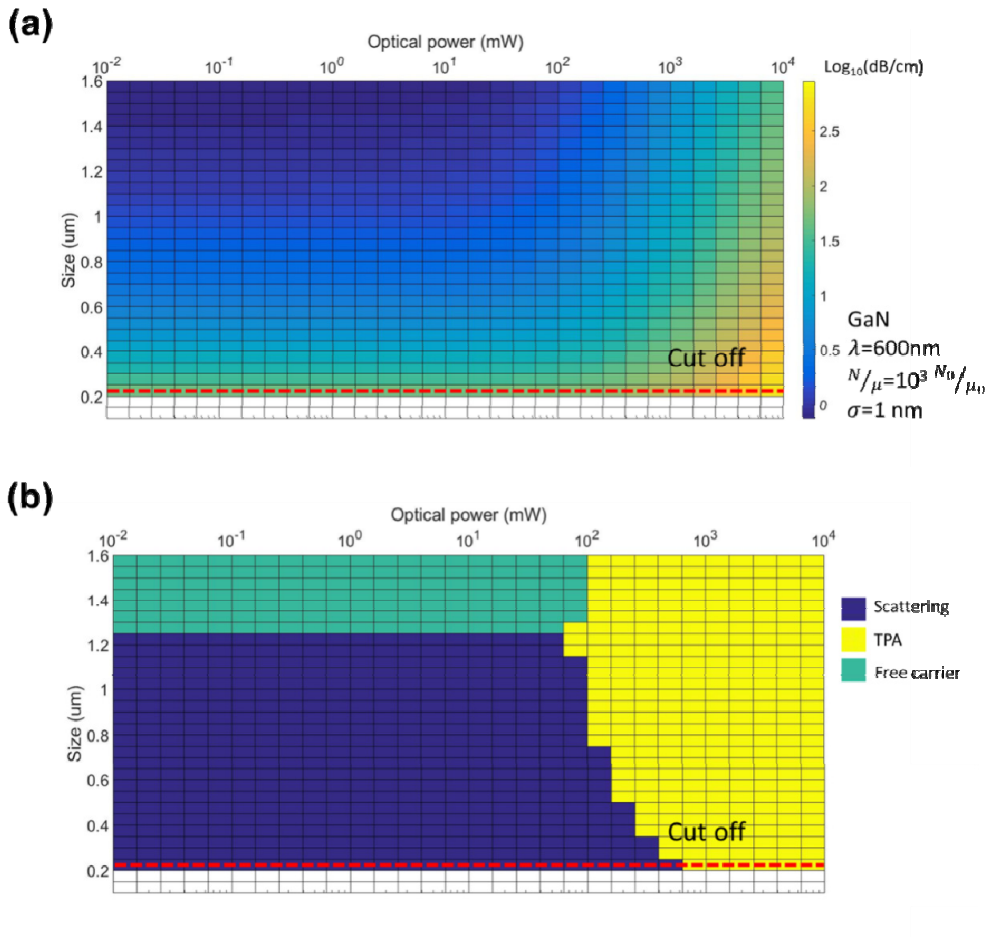

Fig. 6. (a) Calculated loss map of GaN waveguides at 600 nm in a more realistic case, i.e., moderate material quality ($N/\mu = 10^3 N_0/\mu_0$) and sidewall surface roughness σ = 1 nm. (b) Contributions of different loss mechanisms in this GaN waveguide structure. The dashed line in both plots refers to the mode cut off.

3. Experimental results

In this section, we discuss our experimental work on the fabrication and characterization of low loss GaN waveguides. The experimental results show that TPA loss dominates at high incident power range, which is consistent with our calculation results. High performance GaN waveguides with optical loss as low as ~2dB/cm are achieved above half bandgap energy ($\lambda <$ 770 nm), which is the lowest value ever reported for GaN waveguides at this wavelength spectral range.

3.1 Fabrication and testing methods

Figure 7 shows the fabrication process for GaN-on-sapphire waveguide developed for this work. An unintentionally dope (UID) GaN thin film with 1.5 μm thickness was grown on a sapphire substrate using a standard metal organic chemical vapor deposition (MOCVD) process. The Ga and N sources were trimethylgallium and ammonia, respectively. The carrier gas was hydrogen. Surface roughness was measured by atomic force microscope (AFM) and the root mean square (RMS) of height is typically 3.5 nm over 5 μm × 5 μm. 700 nm SiO_2 and 30 nm Cr layers were deposited using plasma-enhanced chemical vapor deposition

Optics EXPRESS

(PECVD) and thermal evaporation, respectively. The SiO_2 layer was used as hardmask for GaN etching. Cr served as a hardmask and also provided conductivity during exposure in electron beam lithography (EBL).

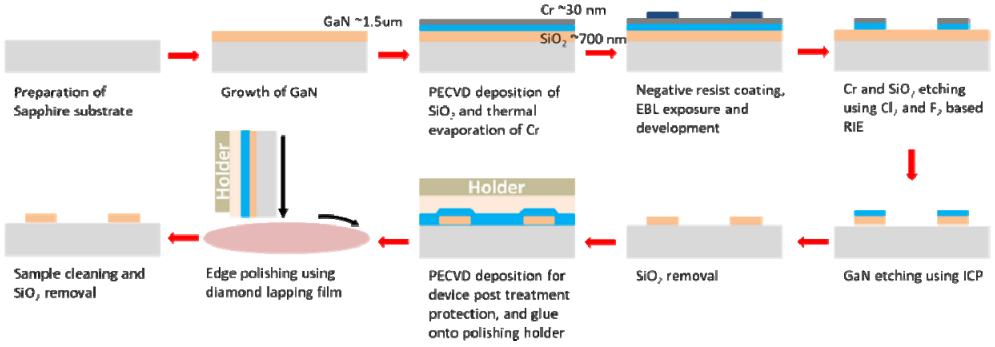

Fig. 7. Fabrication process of GaN-on-sapphire waveguides.

The samples were then coated with a negative resist (ma-N 2403) from Micro Chem Corporation. Then, patterns were transferred to the samples by EBL, where the exposure was intentionally slightly overdosed to reduce sidewall roughness. After EBL exposure, samples were developed for 35 seconds in ma-D 525 developer, followed by chlorine (Cl_2) and fluorine (F_2) based reactive ion etching (RIE) to define the Cr and SiO_2 hardmasks, respectively. The chlorine based RIE was performed under 100 mT chamber pressure and 20 V bias voltage, which produce isotropic etching profile with etching speed of ~40 nm/min. Due to the thin Cr thickness, this isotropic etching does not give much undercut but minimize the sidewall damage (roughness) of hardmask. While for the fluorine based RIE, the etching was performed under 20 mT pressure and 520 V bias voltage. Good anisotropy was achieved with etching speed of ~40 nm/min. Finally, an inductively coupled plasma (ICP) etching was used to form the waveguide structure. The ICP etching of GaN was also optimized following [48] to minimize side wall roughness with 400 W ICP power, 70W RIE power and 5 mT pressure using 30 sccm Cl_2, 8 sccm BCl_3 and 5 sccm Ar_2. Bias voltage during etching was ~160 V and etching speed was ~200 nm/min. After ICP etching, residual SiO_2 was removed by one hour ultra etch 20:1 NP selective wet etching.

Optics EXPRESS

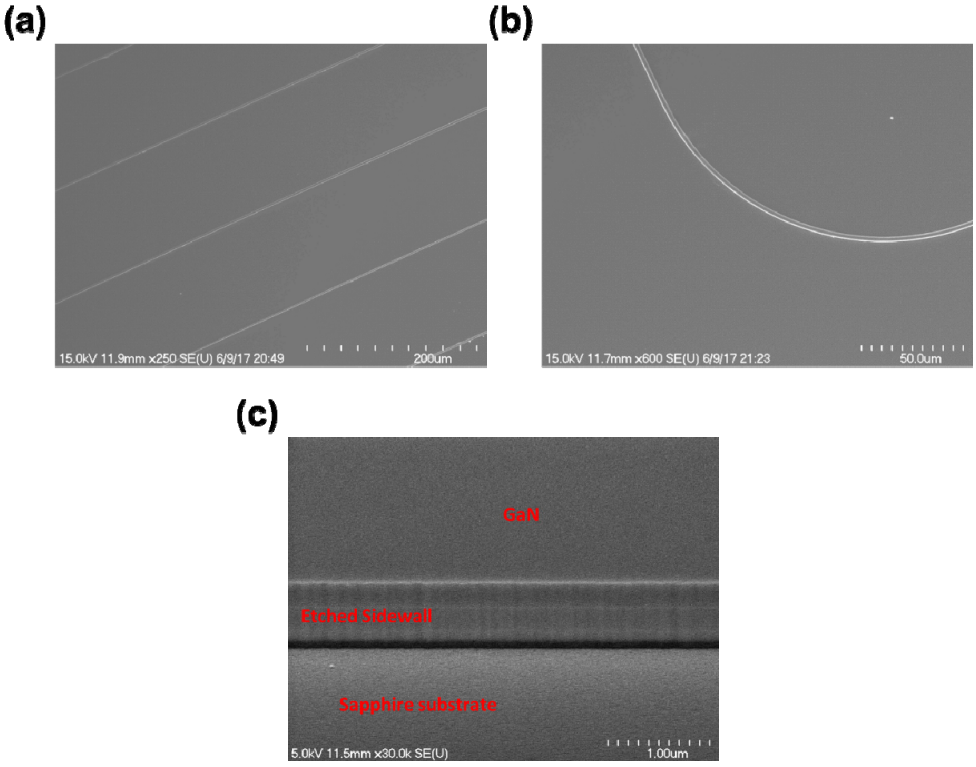

Fig. 8. (a) and (b) SEM images of fabricated GaN-on-sapphire waveguides. (c) SEM image showing the smooth sidewall profile for the GaN waveguides with optimized etching processes.

The scanning electron microscopy (SEM) images of devices are shown in Figs. 8(a) and 8(b). By collecting scattering light and measuring the decay, waveguide loss can be extracted. Figure 8(c) shows the SEM image of a typical sidewall profile for GaN waveguides with optimized etching process. A smooth sidewall profile was obtained using optimized etching processes, where RIE/ICP power were balanced and bias voltage was sufficiently high. Sidewall angle of the etched surface is estimated to be ~70° using the vertical and lateral profile obtained by Dektak stylus profiler and SEM images.

In order to couple light into waveguide, end-fire coupling method was employed. A laser beam from Ti:S laser in TE polarization was first expanded by free space optics to fully utilize the numerical aperture and then focused by a × 10 objective lens. The beam diameter was estimated to be ~2 μm using simple Gaussian optics estimation. Facet of waveguide was tapered to match the beam size of Gaussian laser beam coming out from objective. During testing, the facet of waveguide was positioned at focal point of the objective lens to achieve maximum power injection. The coupling efficiency was calculated to be ~30%.

The tapered facet of the GaN waveguide was polished to further enhance coupling efficiency. Before polishing, a SiO_2 layer was deposited to protect the waveguide during polishing. Samples were glued onto a holder and polished by diamond lapping film, after which the glue and SiO_2 were removed. To test loss of the GaN waveguide, light was guided to propagate inside the waveguide for several millimeters and the scattering light was collected by the microscope and sent to a linear CCD camera. This setup is standard in loss characterization of waveguides and has been widely used [28,49,50]. During experiment, gain of CCD camera was dynamically changed in order to avoid saturation of each pixel. By measuring the decay, waveguide optical loss can be extracted.

Optics EXPRESS

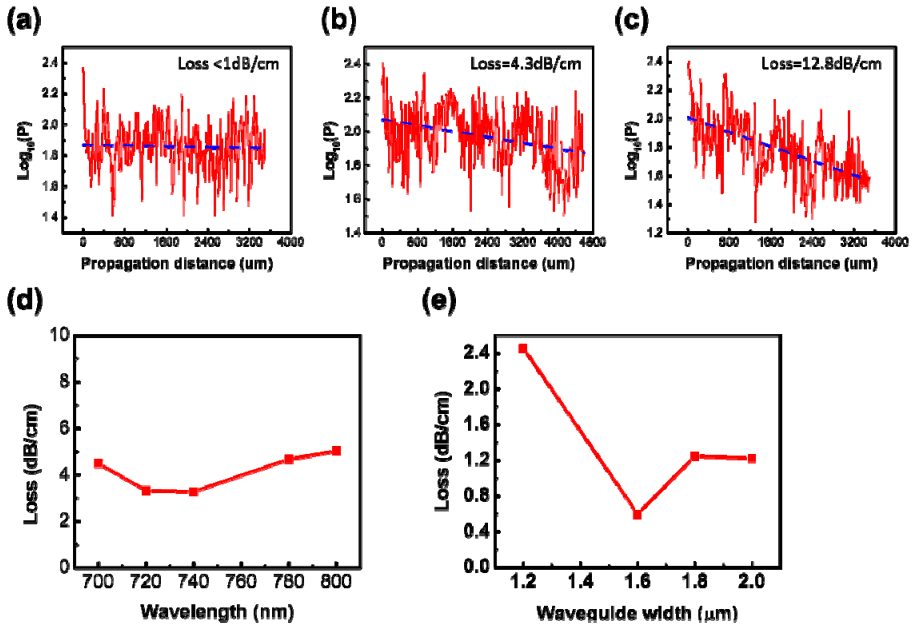

Fig. 9. (a), (b), and (c) Loss characterization of GaN waveguides with good, decent, and failed performance, respectively. The width for each waveguides are 1.6 μm. (d) Loss vs. wavelengths for the GaN waveguide with 1.6 μm width. (e) Loss vs. waveguide width tested at 700 nm in CW lasing mode.

3.2 Results and discussion

Using the process developed in Fig. 7, we fabricated the GaN waveguides with 1.5 μm height and width varying from 1.2 μm to 2 μm. The experimental data of waveguides tested in this study with good, decent, and failed performances are shown in Figs. 9(a), 9(b), and 9(c), respectively. Testing was performed with 700 nm CW light. For a waveguide with decent performance, only small decay happens after propagation of millimeters. While for a typical failed waveguide, large decay (> 10 dB/cm) can be observed in less than 1 cm propagation. The low loss waveguide in this study is defined to be waveguides that exhibits < 10 dB/cm loss since such waveguides are widely used in ring resonator fabrications [7,12–16,20]. Figure 9(d) shows the waveguide loss as a function of wavelength under CW mode incident light with waveguide width of 1.6 μm. Since the waveguides fabricated in this study are above submicron, they showed very weak wavelength dependence in this wavelength region. The width dependence of optical loss is shown in Fig. 9(e), due to the inaccuracy of out scattering characterization method and limited sample length using EBL process, the characterized waveguide loss fluctuates below 2 dB/cm, therefore the trend is not very clear. In this study, 30 total waveguides were characterized. 70% of the waveguides show optical loss of < 10 dB/cm and 20% exhibit loss of ~2 dB/cm. To the best of our knowledge, this value (~2dB/cm) is the lowest loss ever reported on GaN-based waveguides [23,24], and are comparable to the performance of state-of-the-art InP and Si waveguides at 1.55 μm. These low loss GaN waveguides are capable to handle various applications such as Mach-Zehnder (MZ) interferometers, MZ modulators, and high-quality ring resonators.

Table 2 summarize the optical loss performance of recent studies on GaN waveguides. Overall the reported loss values decreases with decreasing wavelengths, indicating that the dominant loss mechanism for GaN waveguide is the scattering loss, as the free carrier loss will increase with increasing wavelength. Comparing with previous studies [23,30,50,51], the GaN waveguides in this work showed the lowest optical loss value (~2.5 dB/cm) with comparable waveguide dimensions. Furthermore, the devices in this work was also tested at a

Optics EXPRESS

shorter wavelength (~700 nm). These results clearly show the high potential for GaN waveguides especially for visible and even UV wavelengths, which is currently unattainable for conventional Si or III-V waveguides. Better performance can be expected from GaN waveguides with further optimized material qualities and fabrication processes.

Table 2. Previous reports on GaN based waveguides

Loss	Waveguide dimension (Width×Height) in μm	Wavelength (nm)	Ref.
Waveguide loss in channel waveguides			
33.4 dB/cm	3 × 3	1559	Hui et al. (2003) [23]
26, 22 dB/cm	0.73 × 0.625	406, 1550	Sekiya et al. (2015) [50]
20 dB/cm	1 × 0.8	1550	Li et al. (2015) [51]
15.2, 5.9 dB/cm	1 × 0.65	775, 1550	Bruch et al. (2015) [30]
2.5 dB/cm	**1.2 × 1.5**[1]	**700**	**This work**
Waveguide loss in planar or bulk waveguides[2]			
0.61 dB/cm	Bulk	1550	Geiss et al. (2005) [52]
4.2, 0.65 dB/cm	Planar (1.5 μm)	830, 1550	Stolz et al. (2011) [24]
1.9 dB/cm	Planar (1 μm)	632.8	Gromovyi et al. (2014) [53]

1. Waveguide with 2.5 dB/cm loss at 1.2 μm × 1.5 μm dimension is picked in this comparison, lower loss can be obtained at wider width.

2. Thin film thickness is given in the bracket.

The low loss performance from the GaN waveguides can be attributed to the optimized ICP dry etching process that minimizes the sidewall roughness of the devices. The loss variation of the waveguides across the wafer can be attributed to several reasons. Firstly, SiO_2 cracking was observed on some area of the wafer, possibly due to large thermal expansion coefficient difference between SiO_2 and GaN. The cracking of SiO_2 hardmask could result in the damage of waveguide in the device etching steps. Secondly, the mechanical polishing process could cause damage to some waveguides. For the former issue, we can optimize the PECVD deposition process and/or use thinner SiO_2 layers to avoid non-ideality and cracking. For the latter issue, grating couplers can be employed to eliminate the polishing process. Further improvements of the GaN waveguide are expected by optimizing the growth and fabrication process.

In order to verify that TPA loss is the dominated optical loss mechanism for GaN waveguide at the visible spectral range under strong power incidence, we further characterized the waveguide under pulsed laser mode. During the testing, a 100-fs laser pulsed at 82 MHz repetition rate was utilized with operating wavelength of 710 nm. The loss of the GaN waveguide with height of 1.5 μm and width of 2 μm was characterized at different incident power under both pulsed and CW mode, and the results are shown in Fig. 10. Under pulse mode, the optical loss of the waveguide showed a strong dependence on the incident power. In contrast, the optical loss was almost constant under CW model over the measured power range. Since TPA loss is power related, it will increase with increasing incident optical power. In comparison, scattering loss and free carrier loss have less power-dependence. Therefore, under pulsed mode operation, the dominant loss mechanism for GaN waveguide is the TPA loss. While for waveguide under CW mode operation, the peak optical power density is much smaller compared with that in pulsed mode, and we do not observe significant power-dependence.

Optics EXPRESS

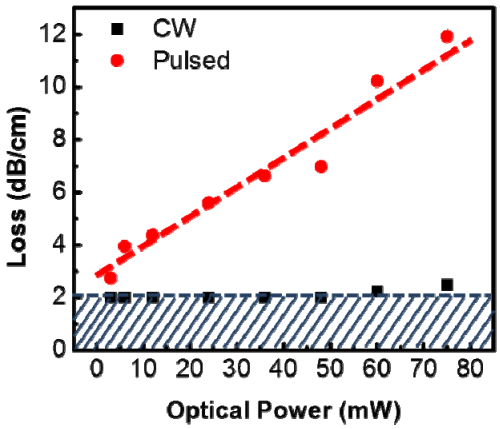

Fig. 10. Loss vs. incident power for the GaN waveguides when the laser is in CW and pulsed mode. Data in the dash line region indicates that the loss is lower than 2 dB/cm.

4. Conclusions

In conclusion, we performed a comprehensive study on the optical loss mechanisms in GaN waveguides at visible spectral range. The results showed that the free carrier loss dominates for GaN waveguides when under low power operation, which is different from traditional InP or Si waveguides working at 1550 nm where scattering loss dominates. Under high power operation, TPA loss starts to dominate for GaN waveguides. A high performance GaN-on-sapphire waveguide was fabricated and characterized, and the experimental results are consistent with the theoretical findings. A low optical loss ~2 dB/cm was achieved on the GaN waveguide, which is the lowest value ever reported for the visible spectral range. The results and fabrication processes developed in this work pave the way for the development of III-nitride integrated photonics in the visible and potentially ultraviolet spectral range for nonlinear optics and quantum photonics applications.

Funding

Science Foundation Arizona.

Acknowledgments

The authors thank Dr. Michael Gerhold of US Army Research Office for the helpful discussion. This work is supported by the Bisgrove Scholar Program from Science Foundation Arizona. We gratefully acknowledge the use of facilities within the LeRoy Eyring Center for Solid State Science and CLAS Ultra Fast Laser Facility at Arizona State University. The author would like to thank Dr. Douglas Daniel, Dr. Lin Gan and Dr. Su Lin for the helpful assistance during experiment. The authors also thank Shi Chen, Jiabi Xiong, and Yaxiao Lai of Wuhan National Laboratory for Optoelectronics for the discussion.